



RESEARCH LETTER

10.1002/2014GL061231

Key Points:

- *P* wave and *S* wave mantle tomography spanning the contiguous U.S.
- Passive margin low-velocity anomalies linked to Cenozoic and Mesozoic volcanism
- Some Laramide-age slab fragments have yet to sink into the lower mantle

Supporting Information:

- Readme
- Figures S1–S3

Correspondence to:

B. Schmandt,
bschmandt@unm.edu

Citation:

Schmandt, B., and F.-C. Lin (2014), *P* and *S* wave tomography of the mantle beneath the United States, *Geophys. Res. Lett.*, 41, doi:10.1002/2014GL061231.

Received 16 JUL 2014

Accepted 6 SEP 2014

Accepted article online 11 SEP 2014

P and *S* wave tomography of the mantle beneath the United States

Brandon Schmandt¹ and Fan-Chi Lin²

¹Department of Earth and Planetary Sciences, University of New Mexico, Albuquerque, New Mexico, USA, ²Department of Geology and Geophysics, University of Utah, Salt Lake City, Utah, USA

Abstract Mantle seismic structure beneath the United States spanning from the active western plate margin to the passive eastern margin was imaged with teleseismic *P* and *S* wave traveltime tomography including USArray data up to May 2014. To mitigate artifacts from crustal structure 5–40 s, Rayleigh wave phase velocities were used to create a 3-D starting model. Major features of the final *P* and *S* models include two distinct low-velocity anomalies at depths of ~60–300 km beneath the central and northern Appalachians and passive margin. The central Appalachian low-velocity anomaly coincides with Eocene basaltic magmatism, and the northern anomaly is located along the Cretaceous track of the Great Meteor hot spot. At depths of ~300–700 km beneath the central and eastern U.S. large high-velocity anomalies are inferred to be remnants of the Farallon slab that subducted prior to ~40 Ma during the Laramide orogeny.

1. Introduction

Arrival of the EarthScope program's USArray network of seismometers on the northeastern coast of the U.S. in Fall 2013 provides seismic sampling spanning from the active western plate margin to the passive eastern plate margin (Figure 1). The emerging data afford new opportunities to study North America's cratonic and passive margin lithosphere and underlying mantle convection. Most of the Laurentian craton was assembled by ~1.5 Ga [Hoffman, 1988; Whitmeyer and Karlstrom, 2007]. Its margins were modified and expanded during two subsequent supercontinent cycles that included the assembly of Rodinia, opening and closing of the Iapetus Ocean, and assembly of Pangea [Whitmeyer and Karlstrom, 2007; Hynes and Rivers, 2010; Hatcher, 2010]. Opening of the Atlantic Ocean started at ~200 Ma [Hames et al., 2000; Blackburn et al., 2013] and the East Coast was established as a passive margin by ~180 Ma [Faill, 1998]. Subsequent geodynamic activity in the eastern U.S. reflects postorogenic evolution of continental lithosphere and evolving basal boundary conditions imposed by mantle convection rather than active plate margin processes.

The passive margin hosted localized magmatic events in the Mesozoic [e.g., Heaman and Kjarsgaard, 2000; Heaman et al., 2004] and Cenozoic [Mazza et al., 2014], and sedimentary and geomorphic studies indicate landscape disequilibrium along the Appalachian mountain belt continuing to the present [e.g., Pazzaglia and Gardner, 2000; Galen et al., 2013; Miller et al., 2013]. The importance of different potential driving forces for passive margin evolution is not well understood. Postorogenic processes such as deep crustal metamorphism [Fischer, 2002] and delamination [e.g., Nelson, 1992] can redistribute mass at depth and the latter may stimulate localized episodes of volcanism [e.g., Elkins-Tanton, 2007; Zandt et al., 2004]. Alternatively, small-scale upper mantle convection and volcanism may be organized by proximity to the edge of the cold tectospheric root landward of the Precambrian rift margin [e.g., King, 2007]. Localized mantle upwelling during hot spot volcanism in the Cretaceous may also have modified the passive margin lithosphere in the Cretaceous and influence present-day mantle heterogeneity [Heaman and Kjarsgaard, 2000; Eaton and Frederiksen, 2007; Villemaire et al., 2012; Chu et al., 2013].

Deeper mantle heterogeneity, such as sinking slabs in the transition zone and lower mantle, can affect the surface at longer lateral wavelengths. Mantle convection cells associated with sinking of slabs in the lower mantle beneath the central and eastern U.S. contribute to late Cenozoic topography and erosion [Rowley et al., 2013; Spasojevic et al., 2008; Liu, 2014]. Aside from their influence on thermally driven convection deep slabs may also affect the passive margin by ascent of volatile-rich mantle above sinking slabs, which could alter upper mantle rheology beneath the passive margin [van der Lee et al., 2008]. The influence of slabs deep beneath the eastern U.S. identifies a potential link between modern dynamics of the eastern U.S. and

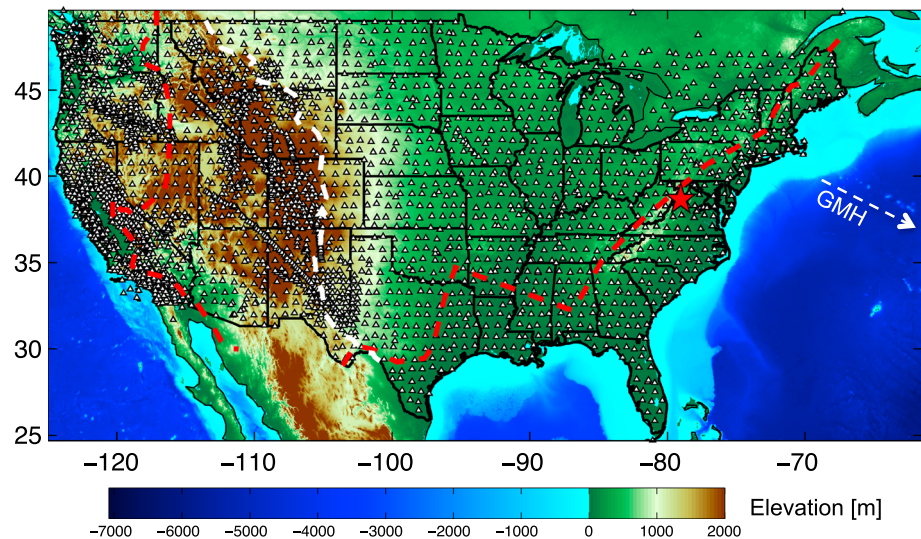


Figure 1. Map of the study area. White triangles with black edges denote seismographs used for body wave traveltime measurements. Red dashed lines indicate the approximate location of Precambrian rift margins of the continent inferred by *Whitmeyer and Karlstrom* [2007]. The white dashed line denotes the Rocky Mountain front, which is the eastern limit of most Cenozoic tectonic and magmatic activity in the western U.S. The red star marks the location of the most recent magmatic event along the passive margin, which occurred at ~ 48 Ma [*Mazza et al.*, 2014]. The white dashed line with an arrowhead in the Atlantic Ocean lies just south of the track of seamounts (~ 80 – 100 Ma) attributed to the Great Meteor hot spot [*Duncan*, 1984; *Heaman and Kjarsgaard*, 2000].

Mesozoic-to-Cenozoic subduction at the western plate margin that drove widespread deformation and magmatism in the North American Cordillera.

Here we present new *P* wave and *S* wave tomography models with coverage across the continental U.S. mantle. Incorporation of USArray data from the eastern U.S. affords new views of lateral heterogeneity along the passive margin. The advance in data coverage also refines prior imaging of structures in the transition zone and top of the lower mantle. We find that low-velocity anomalies in the shallow upper mantle are correlated with Mesozoic and Cenozoic passive margin volcanism and that some slab fragments subducted during the Laramide orogeny (~ 40 – 80 Ma) have not yet sunk into the lower mantle.

2. Data and Methods

The tomography models we present are a major expansion of the *P* and *S* tomography presented by *Schmandt and Humphreys* [2010]. The only methodological difference is that we use a surface wave tomography model of the crust and uppermost mantle as a starting model for the inversion. The data for the surface wave inversion are Rayleigh wave phase velocity maps derived from ambient noise interferometry. We use phase velocity maps from two types of data analysis. The first type is derived from spectral analysis of ambient noise cross correlations and a ray-based inversion for Rayleigh wave phase velocity maps from 5 to 40 s [*Ekström et al.*, 2009; *Ekström*, 2013]. The second type is derived from time domain analysis of noise cross correlations [*Bensen et al.*, 2007] and inverted for phase velocity maps from 8 to 40 s using Eikonal tomography [*Lin et al.*, 2009]. At periods where results from both approaches are available, we use the average. The spatial correlation between the two types of phase velocity maps is consistently ≥ 0.8 , so choosing either method instead of averaging the two would not substantially change our results. Both types of Rayleigh wave phase velocity maps used USArray data through the end of 2013.

The surface wave inversion used three crustal layers and one upper mantle layer underlain by the AK135 reference model [*Kennett et al.*, 1995]. The upper crust layer extends from the surface to 7 km depth, the middle crust layer from 7 to 15 km, and the lower crust layer from 15 km to the local Moho. The upper mantle layer extends from the Moho to 100 km depth. This simple parameterization is adequate to prevent the leakage of crustal structure into the mantle. More detailed aspects of crustal structure could be addressed in

future studies through joint inversion of multiple measurements including surface wave dispersion, Rayleigh wave horizontal/vertical amplitude ratios, and P_s receiver functions [e.g., *Shen et al.*, 2013a; *Lin et al.*, 2014]. The prescribed Moho interface follows the Crust1.0 model [*Laske et al.*, 2013], except in the southwestern U.S. where a higher-resolution model [*Tape et al.*, 2012] is smoothly graded into Crust1.0 (see supporting information). For each location, we perform a 1-D inversion by iteratively applying a sparse least-squares solver [*Paige and Saunders*, 1982] with sensitivity kernels updated between iterations using the Mineos normal mode package [*Masters et al.*, 2007]. For Mineos calculations P velocity and density parameters were prescribed as functions of S velocity following the empirical fit equations 1 and 9 of *Brocher* [2005].

The body wave inversion includes relative traveltimes from USArray data up to May 2014 and additional data from temporary arrays and regional networks as described by *Schmandt and Humphreys* [2010]. Traveltime residuals were measured by multichannel cross correlation [*VanDecar and Crosson*, 1990] in multiple frequency bands with center frequencies of 1, 0.5, 0.33, and 0.1 Hz for P waves and 0.4, 0.1, and 0.05 Hz for S waves. The new P wave and S wave models use 516,688 P and PKP traveltimes and 223,462 S and SKS traveltimes, respectively. The starting crust model inverted from Rayleigh wave measurements was held fixed in the body wave inversion, but we allow the uppermost mantle portion of the starting model to vary. Horizontal grid spacing is 40 km beneath the array interior and expands to 60 km beyond the edges of the array. Vertical grid spacing smoothly increases from 30 km in the uppermost mantle to 70 km at depths greater than 1000 km.

3. Results

The final P and S tomography models provide a good fit to the 5–40 s Rayleigh wave phase velocities as well as teleseismic P wave and S wave residual times measured in multiple frequency bands. The starting model derived from inversion of Rayleigh wave phase velocities achieves a mean misfit to the Rayleigh wave phase velocity measurements of 0.035 km/s. For the final model, after inversion of the S wave traveltime residuals is allowed to modify the upper mantle velocity structure, the mean misfit to the Rayleigh wave phase velocity data increased to 0.043 km/s. Changes to uppermost mantle velocities as a result of the body wave inversion were 0.095 km/s on average, which is similar to estimates of uncertainty in uppermost mantle velocity for a surface wave inversion using USArray data [*Shen et al.*, 2013a]. The final tomography models achieve variance reductions of 70% and 75% for the P wave and S wave residual times, respectively. Following *Schmandt and Humphreys* [2010], we calculated a “hit quality” index for each parameter in the tomography model. This index ranges from 0 to 1 and reflects the azimuthal diversity of ray paths sampling each model parameter. The variance reduction statistics above were calculated only with respect to model parameters that have a hit quality >0.33 , which implies ray paths spanning at least 120° of azimuth. Complete digital models and an interface for making maps and cross sections will be publicly available through Incorporated Research Institutions for Seismology (IRIS) Earth Model Collaboration (www.iris.edu/dms/products/emc/), and images from a resolution test are presented in the supporting information. Major features of the models are introduced below.

Prior USArray tomography studies have presented many features of the western and central U.S. [e.g., *Porritt et al.*, 2014; *Pollitz and Mooney*, 2014; *Schmandt and Humphreys*, 2010; *Obrebski et al.*, 2011; *Burdick et al.*, 2014; *Sigloch*, 2011; *Shen et al.*, 2013a, 2013b; *Evanzia et al.*, 2014]; so, here we focus on newly resolved heterogeneity in the shallow upper mantle near the passive margin and improved imaging of deeper anomalies in the transition zone and lower mantle. High velocities are generally imaged in the uppermost mantle landward of the eastern Precambrian rift margin (Figure 2). At the southern edge of the array, low-velocity mantle reaches farther inland and approximately follows the Precambrian rift margin beneath the Mississippi Embayment [*Yuan et al.*, 2014; *Pollitz and Mooney*, 2014]. Uppermost mantle (~75 km) velocities beneath the passive margin are generally intermediate to those of the craton and the western U.S. Cordillera (Figures 2a and 2b). However, there is considerable along-strike heterogeneity beneath the passive margin.

We specifically note two distinct low-velocity anomalies that underlie the central and northern Appalachian mountain belt and adjacent coast. The central Appalachian anomaly is about 70–100 km wide at 75 km depth, more prominent in the S model compared to the P model, and it is centered beneath northwestern Virginia (Figure 2). At the same depth the northern Appalachian anomaly is about 400 km wide and it underlies Massachusetts, Vermont, and New Hampshire (Figure 2). The northern feature was previously reported by tomography studies with the sparse data coverage that existed prior the arrival of USArray in the

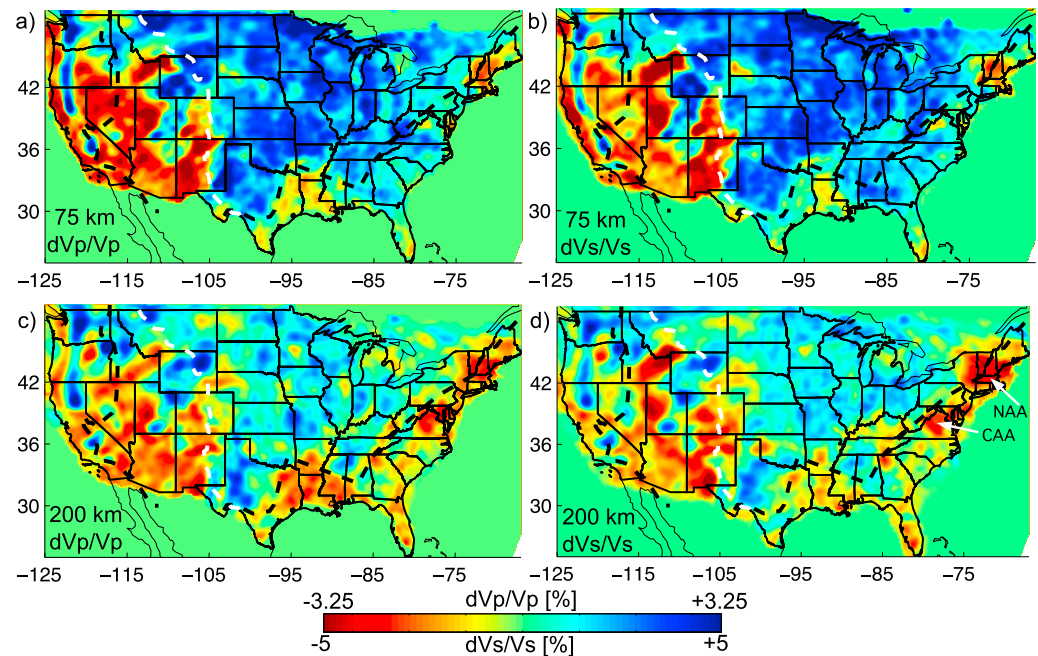


Figure 2. Tomography maps of the shallow upper mantle. (a) P wave tomography at a depth of 75 km. The black dashed lines indicate Precambrian rift margins adapted from *Whitmeyer and Karlstrom* [2007], and the white dashed line denotes the Rocky Mountain front. The locations of the central Appalachian anomaly (CAA) and northern Appalachian anomaly are labeled in Figure 2d. (b) S wave tomography at 75 km depth. (c) P wave tomography at 200 km depth. (d) S wave tomography at 200 km depth.

northeastern U.S. [*Eaton and Frederiksen, 2007; Villemaire et al., 2012*]. Both the central and northern Appalachian anomalies widen at depths of 125–200 km, and it is unknown whether these features extend offshore beneath the Atlantic Ocean. The amplitude of both anomalies is strongly diminished at depths greater than ~ 300 km.

Large high-velocity anomalies are imaged at approximately mantle transition zone depths, 410–660 km, and in the lower mantle beneath the central and eastern U.S. Two distinct high-velocity fragments are shown in a horizontal slice through the middle of the transition zone (Figure 3a). A recent study by *Porritt et al.* [2014] also shows these prominent high-velocity features at depths of ~ 300 –700 km. Near the top of the lower mantle, ~ 700 –1200 km depth, high-velocity anomalies are imaged beneath the western Great Plains and eastern Cordillera (-110° to -100° longitude) and beneath the eastern U.S. (-94° to -78° Longitude). In some locations the high-velocity anomaly beneath the eastern margin is overlain by low-velocity mantle similar to earlier tomography models (Figure 3) [*van der Lee et al., 2008; Sigloch, 2011*]. The low-velocity anomalies we image just above the high-velocity anomaly in the lower mantle are generally more segmented compared to prior images.

4. Discussion

4.1. Structural Legacy of Passive Margin Volcanism

At depths of ~ 60 –100 km the central Appalachian low-velocity anomaly coincides with an Eocene (~ 47 Ma) swarm of basaltic volcanism [*Mazza et al., 2014*]. This magmatic event was recently hypothesized to be a consequence of postorogenic delamination that occurred approximately 150 Ma after the opening of the Atlantic [*Mazza et al., 2014*]. Eocene delamination could have left a scar in the thermal lithosphere allowing asthenosphere to locally ascend to shallower depths and create the lateral velocity variations we imaged. An alternative hypothesis for low-velocity upper mantle in this region is thermal erosion of the lithosphere by Cretaceous passage of a hot spot [*Chu et al., 2013*]. Our images of a localized and approximately circular low-velocity anomaly at about 75 km depth rather than an elongated swath of low velocities favor the delamination hypothesis, as does the absence of an extensive seamount chain eastward of the anomaly in

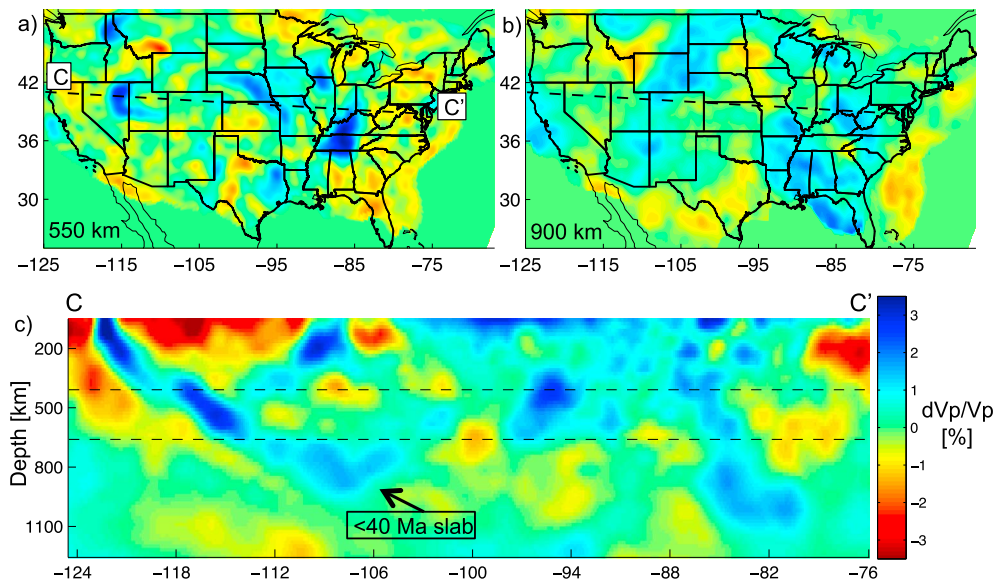


Figure 3. Tomography images of inferred slab remnants. (a) P wave tomography at 550 km depth. The black dashed line indicates the location of the cross section shown in Figure 3c. (b) P wave tomography at 900 km depth. (c) A vertical cross section through the P wave tomography model along the profile labeled C–C' in Figure 3a. The east dipping fragments of high-velocity mantle west of about -105° longitude are interpreted as remnants of subduction beneath the West Coast since ~ 40 Ma, in agreement with forward modeling of mantle convection from Liu and Stegman [2011]. We infer that the high-velocity anomalies farther east at depths greater than 300 km represent older slab fragments that have sunk at slower rates compared to the fragments indicated as <40 Ma.

the Atlantic Ocean. However, westward truncation of the low-velocity anomaly could also be attributed to thicker North America lithosphere west of the Precambrian rift margin (Figure 2). At depths below about 125 km, the low-velocity anomaly widens, extending to the eastern margin of the array (Figure 3c), potentially consistent with lateral encroachment of warmer oceanic asthenosphere beneath the passive margin of North America rather than dominantly vertical ascent of low-velocity mantle.

The northern Appalachian low-velocity anomaly is more laterally extensive than the central Appalachian anomaly at depths of ~ 60 – 100 km, where it spans beneath the states of Massachusetts, Vermont, and New Hampshire (Figure 2). This area overlaps with a P and S receiver function study that indicated a sharp lithosphere-asthenosphere boundary (LAB) manifest as an abrupt 5–10% drop in V_S at ~ 90 – 100 km depth [Rychert *et al.*, 2007]. It is not yet known whether a sharp LAB is confined to the area of the low-velocity anomaly that we image or if it is a widespread feature along the passive margin. Prior interpretations of the northern Appalachian low-velocity anomaly [Villemaire *et al.*, 2012; Eaton and Frederiksen, 2007] focused on the observation that it coincides with the inferred Cretaceous (~ 115 – 130 Ma) track of the Great Meteor hot spot [Heaman and Kjarsgaard, 2000]. A sequence of kimberlite magmatism across Canada [Heaman and Kjarsgaard, 2000] and basaltic magmatism recorded by a chain of seamounts in the Atlantic Ocean [Duncan, 1984] define the Great Meteor hot spot track both northwest and southeast of the northern Appalachian low-velocity anomaly [Villemaire *et al.*, 2012; Eaton and Frederiksen, 2007]. A similar magnitude low-velocity anomaly is not imaged along the inferred hot spot track in the Superior province, which may be an indication that upwelling could not effectively erode the thick lithospheric root of the Superior province [Yuan *et al.*, 2014; Schaeffer and Lebedev, 2014; Chu *et al.*, 2012] or that any Mesozoic thermal erosion of the Precambrian lithosphere has healed sufficiently to avoid detection.

The Great Meteor hot spot provides a plausible trigger for basal erosion of the lithosphere during the Cretaceous, but it leaves a need to understand why such strong seismic heterogeneity exists ~ 100 Ma later. Subsequent small-scale convection driven by proximity to the edge of the Superior craton [e.g., King, 2007] or postorogenic delamination beneath the northern Appalachian Mountains [e.g., Nelson, 1992] are potentially viable processes that could contribute to the low-velocity anomaly that exists today. Seismic imaging of lithospheric discontinuities and mantle anisotropy along the passive margin using USArray data will aid in

constraining postorogenic evolution of the continental lithosphere and ongoing mantle flow beneath the passive margin.

4.2. Slab Remnants Beneath the Central and Eastern U.S.

At depths greater than about 300 km beneath the continent subducted slabs are the only plausible origin for the large volumes of high-velocity mantle that we image because long-period surface wave tomography indicates that the thick keel of cratonic North America remains intact [e.g., *Yuan et al.*, 2014; *Schaeffer and Lebedev*, 2014]. High-velocity anomalies in the lower mantle beneath the eastern U.S. have been long interpreted as remnants of continuous Farallon plate subduction beneath the West Coast [e.g., *Bunge and Grand*, 2000], but high-velocity anomalies at shallower depths of ~300–700 km were not well resolved prior USArray coverage in the eastern U.S. A recently proposed alternative model of Cordilleran evolution incorporates multiple intraoceanic subduction zones west of North America during the Mesozoic [*Sigloch and Mihalynuk*, 2013]. This alternative model assumes uniform slab sinking rates and vertical slab trajectories beneath former trenches in order to predict the origins of high-velocity slabs [*Sigloch and Mihalynuk*, 2013]. While we see merit in the intraoceanic subduction model, our images of large high-velocity fragments beneath the eastern U.S. caution against the assumption of uniform slab sinking rates.

The presence of at least some slab remnants at only ~300–700 km depth beneath the central and eastern U.S. requires strongly variable sinking rates (Figure 3). Regardless of the differences between the intraoceanic subduction model of western plate margin evolution [*Sigloch and Mihalynuk*, 2013] and earlier interpretations [e.g., *Bunge and Grand*, 2000; *Liu et al.*, 2010], the high-velocity anomalies that we image in the transition zone beneath the central and eastern U.S. are farther from potential locations of past subduction zones than some slab fragments beneath the western U.S. that have already sunk into the lower mantle (Figures 3b and 3c). In addition to tomography, *P*-to-*S* receiver function imaging of transition zone thickness also indicates a large volume of relatively cold mantle resides within the transition zone beneath the Great Plains [*Li et al.*, 1998; *Schmandt et al.*, 2012; *Gao and Liu*, 2014].

To estimate a lower bound on the age of the anomalously shallow slab fragments beneath the central and eastern U.S. we consider a recent forward modeling study of western U.S. subduction since 40 Ma [*Liu and Stegman*, 2011]. A first-order fit to tomographically imaged high-velocity anomalies beneath the western U.S. (Figure 3c) was achieved by *Liu and Stegman* [2011] with a numerical convection model coupled to a plate tectonic model since 40 Ma [*Müller et al.*, 2008]. Based on their results, we suggest that the high-velocity anomalies imaged in the transition zone beneath the central and eastern U.S. result from subduction prior to 40 Ma, while the Laramide orogeny was ongoing. Occurrence of low-angle subduction during the Laramide is supported by the inboard extent of deformation and magmatism [e.g., *Coney and Reynolds*, 1977; *Humphreys et al.*, 2003; *Saleeby*, 2003] and the subsidence history of sedimentary basins in the continental interior [*Spasojevic et al.*, 2009]. Our results suggest that the slab involved in low-angle subduction has separated into multiple distinct fragments and that at least two of these large fragments (Figure 3a) have yet to sink into the lower mantle.

Subduction of oceanic plateaus, specifically the inferred conjugates of the Hess and Shatsky plateaus, is a probable trigger for low-angle subduction initiating at ~90 Ma [*Liu et al.*, 2010; *Saleeby*, 2003]. The position of the Hess plateau conjugate predicted by *Liu et al.* [2010] approximately coincides with the high-velocity anomaly we image in the top of the lower mantle beneath the southeastern U.S. at about 900 km depth (Figure 3b). *Liu et al.* [2010] predicted the Shatsky plateau conjugate to be ≥ 1100 km deep and beneath the eastern Great Lakes region. Tomography resolution in that region of the lower mantle will improve significantly with additional data from the northeastern USArray stations and would also benefit from incorporation of additional data from Canada. Consequently, we refrain from comparing the predicted Shatsky conjugate location to our tomography model at this time.

Farallon slab remnants may be important to the origin of low-velocity anomalies in the upper mantle beneath the eastern U.S. Ascent of volatiles from Farallon slab remnants in the lower mantle was previously hypothesized as the origin of low-velocity anomalies beneath the passive margin [*van der Lee et al.*, 2008]. A key aspect to testing this hypothesis is ability to rule out thermal variations as an adequate physical origin for the velocity anomalies. Based on *P* and *S* tomography alone, thermal perturbations are plausible because the *S* anomalies are generally a factor of 1.5–2 greater than the *P* velocity anomalies in the shallow upper

mantle beneath the passive margin (Figure 2) [Cammarano *et al.*, 2003]. Prior studies of the mantle transition zone based on Ps receiver functions [Li *et al.*, 1998; Long *et al.*, 2010] and ScS reverberations [Courtier and Revenaugh, 2006] found that transition zone thickness beneath the eastern U.S. is generally within 10 km of the global average indicating temperatures near the average mantle adiabat. Investigations of transition zone topography using USArray data will better identify lateral variations in transition zone structure [e.g., Gao and Liu, 2014] and provide a stronger basis for assessing the origin of low-velocity anomalies beneath the passive margin. More integrative investigation of the isotropic and anisotropic properties of the anomalies is warranted for general understanding of the effects of deep slabs on the surrounding mantle and specifically for understanding how mantle convection has influenced geological evolution of the eastern U.S. passive margin.

Acknowledgments

Seismic waveform data used in this research are publicly available for download through the IRIS DMC (<http://www.iris.edu/dms/nodes/dmc/>), SCEDC (<http://www.data.scec.org/>), NCEDC (<http://quake.geo.berkeley.edu/>), and CNDC (<http://www.earthquakescanada.nrcan.gc.ca/>). We appreciate the efforts of two anonymous reviewers and the Editor. We thank Goran Ekström for sharing his most recent Rayleigh wave phase velocity maps. The University of New Mexico (B.S.), NSF EAR-1315856 (B.S.), and the University of Utah (F.L.) provided partial support for this research.

The Editor thanks William E. Holt and one anonymous reviewer for their assistance in reviewing this paper.

References

- Bensen, G. D., M. H. Ritzwoller, M. P. Barmin, A. L. Levshin, F. Lin, M. P. Moschetti, N. M. Shapiro, and Y. Yang (2007), Processing seismic ambient noise data to obtain reliable broad-band surface wave dispersion measurements, *Geophys. J. Int.*, *169*(3), 1239–1260, doi:10.1111/j.1365-246X.2007.03374.x.
- Blackburn, T. J., P. E. Olsen, S. A. Bowring, N. M. McLean, D. V. Kent, J. Puffer, G. McHone, E. T. Rasbury, and M. Et-Touhami (2013), Zircon U-Pb geochronology links the end-Triassic extinction with the Central Atlantic Magmatic Province, *Science*, *340*, 941–945, doi:10.1126/science.1234204.
- Brocher, T. M. (2005), Empirical relations between elastic wavespeeds and density in the Earth's crust, *Bull. Seismol. Soc. Am.*, *95*, 2081–2092, doi:10.1785/0120050077.
- Bunge, H.-P., and S. Grand (2000), Mesozoic plate-motion history below the northeast Pacific Ocean from seismic images of the subducted Farallon slab, *Nature*, *405*, 337–340.
- Burdick, S., R. D. Van Der Hilst, F. L. Vernon, V. Martynov, T. Cox, J. Eakins, G. H. Karasu, J. Tylell, L. Astiz, and G. L. Pavlis (2014), Model update January 2013: Upper mantle heterogeneity beneath North America from travel-time tomography with global and USArray transportable array data, *Seismol. Res. Lett.*, *85*, 77–81, doi:10.1785/0220130098.
- Cammarano, F., S. Goes, P. Vacher, and D. Giardini (2003), Inferring upper-mantle temperatures from seismic velocities, *Phys. Earth Planet. Inter.*, *138*(3–4), 197–222, doi:10.1016/S0031-9201(03)00156-0.
- Chu, R., B. Schmandt, and D. V. Helmberger (2012), Upper mantle P velocity structure beneath the Midwestern United States derived from triplicated waveforms, *Geochem. Geophys. Geosyst.*, *13*, Q0AK04, doi:10.1029/2011GC003818.
- Chu, R., W. Leng, D. V. Helmberger, and M. Gurnis (2013), Hidden hotspot track beneath the eastern United States, *Nat. Geosci.*, *6*, 963–966, doi:10.1038/ngeo1949.
- Coney, P. J., and S. J. Reynolds (1977), Flattening of the Farallon slab, *Nature*, *270*, 403–406.
- Courtier, A. M., and J. Revenaugh (2006), A water-rich transition zone beneath the Eastern United States and Gulf of Mexico from multiple ScS reverberations, in *Earth's Deep Water Cycle*, *Geophys. Monogr. Ser.*, vol. 168, edited by S. D. Jacobsen and S. van der Lee, pp. 181–193, AGU, Washington, D. C.
- Duncan, R. A. (1984), Age progressive volcanism in the New England Seamounts and the opening of the central Atlantic Ocean, *J. Geophys. Res.*, *89*, 9980–9990, doi:10.1029/JB089iB12p09980.
- Eaton, D., and A. Frederiksen (2007), Seismic evidence for convection-driven motion of the North American plate, *Nature*, *446*, 428–431.
- Ekström, G. (2013), Love and Rayleigh phase-velocity maps, 5–40 s, of the western and central USA from USArray data, *Earth Planet. Sci. Lett.*, doi:10.1016/j.epsl.2013.11.022.
- Ekström, G., G. A. Abers, and S. H. Webb (2009), Determination of surface-wave phase velocities across USArray from noise and Aki's spectral formulation, *Geophys. Res. Lett.*, *36*, L18301, doi:10.1029/2009GL039131.
- Elkins-Tanton, L. T. (2007), Continental magmatism, volatile recycling, and a heterogeneous mantle caused by lithospheric gravitational instabilities, *J. Geophys. Res.*, *112*, B03405, doi:10.1029/2005JB004072.
- Evanzia, D., J. Pulliam, R. Ainsworth, H. Gurrrola, and K. Pratt (2014), Seismic Vp & Vs tomography of Texas & Oklahoma with a focus on the Gulf Coast margin, *Earth Planet. Sci. Lett.*, doi:10.1016/j.epsl.2013.12.027.
- Faill, R. T. (1998), A geologic history of the north-central Appalachians. Part 3: The Alleghany orogeny, *Am. J. Sci.*, *298*, 131–179.
- Fischer, K. M. (2002), Waning buoyancy in the crustal roots of old mountains, *Nature*, *417*, 933–936.
- Galen, S. F., K. W. Wegmann, and D. R. Bohnenstiehl (2013), Recent rejuvenation of topographic relief in the southern Appalachians, *GSA Today*, *23*(2), 4–10, doi:10.1130/GSATG163A.1.
- Gao, S. S., and K. H. Liu (2014), Mantle transition zone discontinuities beneath the contiguous United States, *J. Geophys. Res. Solid Earth*, *119*, doi:10.1002/2014JB011253.
- Hames, W. E., P. R. Renne, and C. Ruppel (2000), New evidence for geologically instantaneous emplacement of earliest Jurassic Central Atlantic magmatic province basalts on the North American margin, *Geology*, *28*, 859–862.
- Hatcher, R. D., Jr. (2010), The Appalachian orogen: A brief summary, in *From Rodinia to Pangea: The Lithotectonic Record of the Appalachian Region*, *Geol. Soc. Am. Mem.*, vol. 206, edited by R. P. Tollo *et al.*, pp. 1–19, Geol. Soc. Am., Boulder, Colo.
- Heaman, L. M., and B. Kjarsgaard (2000), Timing of eastern North American kimberlite magmatism: Continental extension of the Great Meteor hotspot track?, *Earth Planet. Sci. Lett.*, *178*, 253–268.
- Heaman, L. M., B. A. Kjarsgaard, and R. A. Creaser (2004), The temporal evolution of North American kimberlites, *Lithos*, *76*, 377–397.
- Hoffman, P. F. (1988), United plates of America, the birth of a craton: Early Proterozoic assembly and growth of Laurentia, *Annu. Rev. Earth Planet. Sci.*, *16*, 543–603, doi:10.1146/annurev.ea.16.050188.002551.
- Humphreys, E., E. Hessler, K. Dueker, C. L. Farmer, E. Erslev, and T. Atwater (2003), How Laramide-age hydration of North American lithosphere by the Farallon slab controlled subsequent activity in the western United States, *Int. Geol. Rev.*, *45*(7), 575–595.
- Hynes, A., and T. Rivers (2010), Protracted continental collision—Evidence from the Grenville Orogen, *Can. J. Earth Sci.*, *47*, 591–620, doi:10.1139/E10-003.
- Kennett, B. L. N., E. R. Engdahl, and R. Buland (1995), Constraints on seismic velocities in the Earth from travel times, *Geophys. J. Int.*, *122*, 108–124.
- King, S. D. (2007), Hotspots and edge-driven convection, *Geology*, *35*, 223–226.

- Laske, G., G. Masters, Z. Ma, and M. Pasyanos (2013), Update on CRUST1.0—A 1-degree global model of Earth's crust, *Geophys. Res. Abstr.*, *15*, Abstract EGU2013-2658.
- Li, A., K. M. Fischer, M. E. Wyssession, and T. J. Clarke (1998), Mantle discontinuities and temperature under the North American continental keel, *Nature*, *395*, 160–163.
- Lin, F.-C., M. H. Ritzwoller, and R. Snieder (2009), Eikonal tomography: Surface wave tomography by phase front tracking across a regional broad-band seismic array, *Geophys. J. Int.*, *177*(3), 1091–1110, doi:10.1111/j.1365-246X.2009.04105.x.
- Lin, F.-C., V. C. Tsai, and B. Schmandt (2014), 3-D crustal structure of the western United States: Application of Rayleigh-wave ellipticity extracted from noise cross-correlations, *Geophys. J. Int.*, doi:10.1093/gji/ggu160.
- Liu, L. (2014), Rejuvenation of Appalachian topography caused by subsidence-induced differential erosion, *Nat. Geosci.*, *7*, 518–523, doi:10.1038/ngeo2187.
- Liu, L., and D. R. Stegman (2011), Segmentation of the Farallon slab, *Earth Planet. Sci. Lett.*, *311*, 1–10.
- Liu, L., M. Gurnis, M. Seton, J. Saleeby, R. D. Müller, and J. M. Jackson (2010), The role of oceanic plateau subduction in the Laramide orogeny, *Nat. Geosci.*, *3*, 353–357, doi:10.1038/NNGEO829.
- Long, M. D., M. H. Benoit, M. C. Chapman, and S. D. King (2010), Upper mantle anisotropy and transition zone thickness beneath southeastern North America and implications for mantle dynamics, *Geochem. Geophys. Geosyst.*, *11*, Q10012, doi:10.1029/2010GC003247.
- Masters, G., M. P. Barmine, and S. Kientz (2007), *Mineos User's Manual, in Computational Infrastructure for Geodynamics*, Calif. Inst. of Technol., Pasadena, Calif.
- Mazza, S. E., E. Gazel, E. A. Johnson, M. J. Kunk, R. McAleer, J. A. Spotila, and D. S. Coleman (2014), Volcanoes of the passive margin: The youngest magmatic event in eastern North America, *Geology*, *42*(6), 483–486.
- Miller, S. R., P. B. Sak, E. Kirby, and P. R. Bierman (2013), Neogene rejuvenation of central Appalachian topography: Evidence for differential rock uplift from stream profiles and erosion rates, *Earth Planet. Sci. Lett.*, *369–370*, 1–12, doi:10.1016/j.epsl.2013.04.007.
- Müller, R. D., M. Sdrolias, C. Gaina, and W. R. Roest (2008), Age, spreading rates and spreading asymmetry of the world's ocean crust, *Geochem. Geophys. Geosyst.*, *9*, Q04006, doi:10.1029/2007GC001743.
- Nelson, K. D. (1992), Are crustal thickness variations in old mountain belts like the Appalachians a consequence of lithospheric delamination?, *Geology*, *20*, 498–502, doi:10.1130/0091-7613(1992)020<0498:ACTVIO>2.3.CO;2.
- Obrebski, M., R. M. Allen, F. Pollitz, and S.-H. Hung (2011), Lithosphere–asthenosphere interaction beneath the western United States from the joint inversion of body-wave traveltimes and surface-wave phase velocities, *Geophys. J. Int.*, *185*, 1003–1021, doi:10.1111/j.1365-246X.2011.04990.x.
- Paige, C. C., and M. A. Saunders (1982), LSQR: An algorithm for sparse linear equations and sparse least squares, *ACM Trans. Math. Software*, *8*, 43–71.
- Pazzaglia, F. J., and T. W. Gardner (2000), Late Cenozoic landscape evolution of the US Atlantic passive margin: Insights into a North American great escarpment, in *Geomorphology and Global Tectonics*, edited by M. A. Summerfield, pp. 284–302, Wiley InterScience, Chichester, U. K.
- Pollitz, F. F., and W. D. Mooney (2014), Seismic structure of the Central US crust and shallow upper mantle: Uniqueness of the Reelfoot Rift, *Earth Planet. Sci. Lett.*, doi:10.1016/j.epsl.2013.05.042.
- Porritt, R. W., R. M. Allen, and F. F. Pollitz (2014), Seismic imaging east of the Rocky Mountains with USArray, *Earth Planet. Sci. Lett.*, doi:10.1016/j.epsl.2013.10.034.
- Rowley, D. B., A. M. Forte, R. Moucha, J. Mitrovica, N. Simmons, and S. Grand (2013), Dynamic topography change of the eastern United States since 3 million years ago, *Science*, *340*, 1560–1563, doi:10.1126/science.1229180.
- Rychert, C. A., S. Rondenay, and K. M. Fischer (2007), P-to-S and S-to-P imaging of a sharp lithosphere–asthenosphere boundary beneath eastern North America, *J. Geophys. Res.*, *112*, B08314, doi:10.1029/2006JB004619.
- Saleeby, J. (2003), Segmentation of the Laramide Slab—Evidence from the southern Sierra Nevada region, *Bull. Geol. Soc. Am.*, *115*, 655–668.
- Schaeffer, A., and S. Lebedev (2014), Imaging the North American continent using waveform inversion of global and USArray data, *Earth Planet. Sci. Lett.*, doi:10.1016/j.epsl.2014.05.014.
- Schmandt, B., and E. Humphreys (2010), Complex subduction and small-scale convection revealed by body-wave tomography of the western United States upper mantle, *Earth Planet. Sci. Lett.*, *297*, 435–445, doi:10.1016/j.epsl.2010.06.047.
- Schmandt, B., K. Dueker, E. Humphreys, and S. Hansen (2012), Hot mantle upwelling across the 660 beneath Yellowstone, *Earth Planet. Sci. Lett.*, *331–332*, 224–236, doi:10.1016/j.epsl.2012.03.025.
- Shen, W., M. H. Ritzwoller, and V. Schulte-Pelkum (2013a), A 3-D model of the crust and uppermost mantle beneath the Central and Western US by joint inversion of receiver functions and surface wave dispersion, *J. Geophys. Res. Solid Earth*, *118*, 262–276, doi:10.1029/2012JB009602.
- Shen, W., M. H. Ritzwoller, and V. Schulte-Pelkum (2013b), Crustal and uppermost mantle structure in the central U.S. encompassing the Midcontinent Rift, *J. Geophys. Res. Solid Earth*, *118*, 4325–4344, doi:10.1002/jgrb.50321.
- Sigloch, K. (2011), Mantle provinces under North America from multifrequency P wave tomography, *Geochem. Geophys. Geosyst.*, *12*, Q02W08, doi:10.1029/2010GC003421.
- Sigloch, K., and M. G. Mihalynuk (2013), Intra-oceanic subduction shaped the assembly of Cordilleran North America, *Nature*, *496*, 50–56.
- Spasojevic, S., L. Liu, M. Gurnis, and R. D. Müller (2008), The case for dynamic subsidence of the United States east coast since the Eocene, *Geophys. Res. Lett.*, *35*, L08305, doi:10.1029/2008GL033511.
- Spasojevic, S., L. Liu, and M. Gurnis (2009), Adjoint models of mantle convection with seismic, plate motion, and stratigraphic constraints: North America since the Late Cretaceous, *Geochem. Geophys. Geosyst.*, *10*, Q05W02, doi:10.1029/2008GC002345.
- Tape, C., A. Plesch, J. H. Shaw, and H. Gilbert (2012), Estimating a continuous Moho surface for the California Unified Velocity Model, *Seismol. Res. Lett.*, *83*, 728–735.
- VanDecar, J. C., and R. S. Crosson (1990), Determination of teleseismic relative phase arrival times using multi-channel cross-correlation and least squares, *Bull. Seismol. Soc. Am.*, *80*, 150–169.
- van der Lee, S., K. Regenauer-Lieb, and D. Yuen (2008), The role of water in connecting past and future episodes of subduction, *Earth Planet. Sci. Lett.*, *273*, 15–27, doi:10.1016/j.epsl.2008.04.041.
- Villemare, M., F. A. Darbyshire, and I. D. Bastow (2012), P-wave tomography of eastern North America: Evidence for mantle evolution from Archean to Phanerozoic, and modification during subsequent hot spot tectonism, *J. Geophys. Res.*, *117*, B12302, doi:10.1029/2012JB009639.
- Whitmeyer, S. J., and K. E. Karlstrom (2007), Tectonic model for the Proterozoic growth of North America, *Geosphere*, *3*, 220–259.
- Yuan, H., S. French, P. Cupillard, and B. Romanowicz (2014), Lithospheric expression of geological units in central and eastern North America from full waveform tomography, *Earth Planet. Sci. Lett.*, doi:10.1016/j.epsl.2013.11.057.
- Zandt, G., H. Gilbert, T. J. Owens, M. Ducea, J. Saleeby, and C. H. Jones (2004), Active foundering of a continental arc root beneath the southern Sierra Nevada in California, *Nature*, *431*, 41–46.